

Article

Structure and Infrared Emissivity Properties of the MAO Coatings Formed on TC4 Alloys in K_2ZrF_6 -Based Solution

Guangrui Gao ^{1,2,3,*} , Ying Li ^{1,*}, Dan Hu ³ and Zhengping Xi ¹

¹ School of Metallurgy, Northeastern University, Shenyang 110819, China; mayanyan0814@163.com

² Northwest Institute for Nonferrous Metal Research, Xi'an 710016, China

³ Xi'an Surface Material Protection Co, Ltd., Xi'an 710016, China; xiansfs@126.com

* Correspondence: 13571490985@126.com (G.G.); liying@mail.neu.edu.cn (Y.L.); Tel.: +86-135-7149-0985 (G.G.); +86-131-9008-6601 (Y.L.)

Received: 16 January 2018; Accepted: 6 February 2018; Published: 7 February 2018

Abstract: Micro-arc oxidation (MAO) ceramic coatings were formed on TC4 alloy surface in silicate and metaphosphate electrolytes based with K_2ZrF_6 for various concentrations. X-ray diffraction (XRD), Scanning electron microscopy (SEM), X-ray photoelectron spectroscopy (XPS) were used to characterize the phase composition, microstructure and chemical compositions of the coatings. The infrared emissivity of the coatings was measured at 50 °C in a wavelength range of 8–20 μm . The microstructural observations all revealed the typical porous structures. Moreover, a decline in roughness and thickness of the prepared coatings can be observed when the concentration of K_2ZrF_6 increases. Combined with the results of XRD and XPS, it was found that all the oxides existed as the amorphous form in the coatings except the TiO_2 phase. The coatings exhibited the highest infrared emissivity value (about 0.89) when the concentration of K_2ZrF_6 was 6 g/L, which was possibly attributed to the defect microstructure and the optimal role of ZrO_2 .

Keywords: micro-arc oxidation; K_2ZrF_6 ; coating; infrared emissivity

1. Introduction

With the development of infrared technology in recent years, the research of high emissivity coatings has become a focus around the world. These coatings have been widely used in various fields such as thermal protection systems and energy-saving in industrial furnace [1–5]. Substances such as carbides (mainly SiC), transition metal oxides (MnO_2 , Fe_2O_3 , ZrO_2 , Cr_2O_3 , NiO, TiO_2 , Co_3O_4 , et al.), as well as ceramics and glass are usually used to prepare high emissivity coatings due to their high infrared emissivity [6,7]. For instance, Li et al. prepared a kind of high infrared emissivity coating by applying the mixture of $ZrSiO_4$ and aluminosilicate glass powder to the SiC matrix, and then treated by high temperature sintering. The average emissivity of the coatings in the waveband of 1–22 μm demonstrated the highest value around of 0.93. Furthermore the coatings also had high temperature oxidation resistance and compactness [8]. Likewise, Tang et al. added $FeSO_4$ into the electrolyte to prepare the micro-arc oxidation (MAO) coatings with high emissivity on TC4 alloys. The emissivity of the coating with 3 g/L $FeSO_4$ reached the maximum 0.87, and its bonding strength was higher than 33 MPa [9].

Up to now, many surface treatment techniques have been adapted to the preparation of high emissivity coatings including brushing, sintering, electro deposition, electroless deposition and sol-gel technique, etc. However, some widespread problems exist such as poor uniformity, low bonding strength and high preparation costs. Micro arc oxidation, also named as Plasma electrolytic oxidation or Micro plasma oxidation, is acknowledged as an advanced surface treatment technology of placing

the valve metals or their alloys in electrolytes under the additional high voltage. During the reaction process, the oxide film on the surface is instantly broken down and the appearance of the sparks leads to the formation of the discharge channel, which makes the ceramic coatings grow in situ through the reaction of the electrolytes and the metal substrate. Compared with the traditional anodization, the MAO technology transforms the working area into a high-pressure discharge zone so as to prepare the ceramic coatings, which could simultaneously achieve high wear resistance, better corrosion resistance and stronger binding strength between the coatings and substrate [10,11]. Furthermore, this technology also has the advantages of high production efficiency and less environmental pollution. In addition, the MAO coatings of different composition can be obtained by adjusting the electrolyte composition and process parameters. Therefore, using the MAO technique to deposit the functional coatings has received much attention in recent years [12–14].

In general, the infrared emissivity of MAO coatings is related to the chemical composition, surface condition, coating thickness, and electrolytic parameters, but the most influential factor is the composition. It is worth noting that zirconium oxide has high thermal stability, oxidation resistance and low specific heat as well as thermal conductivity as a kind of transition metal oxide. Several authors have researched the effect of K_2ZrF_6 on properties of the ceramic coatings. Zhang et al. observed the MAO coatings fabricated on an aluminum alloy which were produced in the K_2ZrF_6 -based electrolyte [15]. The study found that the deposition rate of the coatings and their uniformity all increased obviously by adding K_2ZrF_6 , and the coatings also exhibited the excellent heat resistance. It is further reported by various researchers that K_2ZrF_6 could increase the tensile strength and shear strength of the MAO coatings [16,17]. However, most researches mainly focus on the significant improvement in mechanical properties, thermal shock resistance as well as corrosion resistance of the coatings, and there are few reports about the infrared emission performance [18–20]. In this work, the micro-arc oxidation method was carried out on TC4 alloy substrate under the different concentration of K_2ZrF_6 , the effect of the K_2ZrF_6 additives on the phase composition, microstructure, chemical composition and infrared emissivity was systematically investigated. Meanwhile, this paper also includes a further expatiation about the reaction details.

2. Materials and Methods

TC4 alloy ($Fe \leq 0.30$, $C \leq 0.10$, $N \leq 0.05$, $H \leq 0.015$, $O \leq 0.20$, Al: 5.5–6.8, V: 3.5–4.5, all in wt %) was cut into the regular specimens with dimensions of 30 mm × 30 mm × 2 mm and used as the substrate to be treated. These specimens were ground successively to 1500 grit SiC papers, then ultrasonically rinsed with ethyl alcohol and dried in room temperature. The specimens were used as anode and a electrolyser which made of stainless steel served as cathode. In this work, the MAO process was carried out for 40 min using a 300 kW positive pulsed device and the main pulse parameters were fixed as follows: frequency 600 Hz, voltage 500 V, and a duty cycle of 15%. The reaction temperature was cooled by a cooling water system to control the value between 25 °C–40 °C. The electrolytes were composed of Na_2SiO_3 (10 g/L), $(NaPO_3)_6$ (6 g/L), NaOH (0.8 g/L), with K_2ZrF_6 0 g/L, 3 g/L, 6 g/L, 9 g/L respectively. After the preparation process, all samples were rinsed with distilled water and dried with the blower.

Phase composition of the coatings was analyzed by a RICOH/max-rB automatic X-ray diffractometer (XRD, D/max-2200pc, RIGAKU, Tokyo, Japan) using a Cu $K\alpha$ source. The surface and cross-section morphologies of the MAO treated coatings were observed by scanning electron microscopy (SEM, JSM6460, JEOL, Tokyo, Japan), and the chemical compositions of the coatings were measured by energy dispersive X-ray spectrometer (EDS) attached to SEM. X-ray photoelectron spectroscopy (XPS, ESCALAB 250Xi, Thermo Fisher Scientific, Waltham, MA, USA) with an Al $K\alpha$ anode was utilized to determine the chemical states of the elements. The thickness and roughness of the coatings were respectively measured by eddy current thickness meter (TT 260, Time Company, Beijing, China) and surface roughness tester (TR-200, Time Company, Beijing, China). Fourier transform

infrared (FT/IR-6100, JASCO, Tokyo, Japan) was used to measure the infrared emissivity of the coatings at 50 °C.

3. Results

3.1. Surface and Cross-Section Microstructure

Figure 1 shows the thickness and roughness of the MAO coatings formed in different electrolytes. Three samples were tested in each group, 10 points were selected on each sample and the average was taken as the final measurement data. It can be seen that lower thickness and roughness were obtained with the introduction of K_2ZrF_6 . Furthermore, it can be noted that the thickness did not decline significantly except when the additive quantity of K_2ZrF_6 reached 9 g/L and the roughness markedly dropped when the K_2ZrF_6 concentration is up to 6 g/L. The reason for this may be attributed to the inhibition of K_2ZrF_6 on the deposition of silicate and metaphosphate on the surface of the coatings.

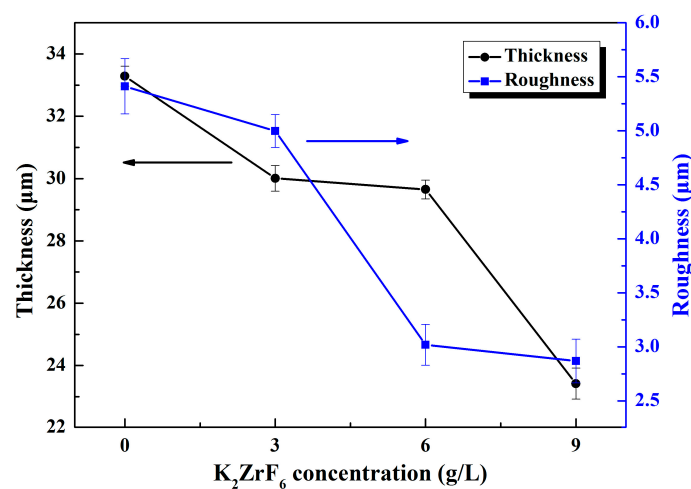


Figure 1. Thickness and roughness of the micro-arc oxidation (MAO) coatings under different K_2ZrF_6 concentrations.

Figure 2 displays the surface morphologies of the MAO coatings prepared under various conditions. All the coatings possess a porous structure with many crater-shaped micro-pores irregularly distributed and the appearance of this structure is due to the molten oxides and the gas bubbles of the discharge phenomena in the processes. In addition, the surface morphologies as shown in Figure 2 exhibit an obvious difference. With an increase in K_2ZrF_6 concentration, the roughness of the coatings decreases, which is consistent with the results of Figure 1. From Figure 2a, large spherical particles with the diameter of several micrometers distribute on the surface. As the concentration of K_2ZrF_6 increase to 3 g/L, some protrusions have a tendency to become smooth as shown in Figure 2b. A clearly transformation occurs when the concentration of K_2ZrF_6 reaches 6 g/L and 9 g/L (Figure 2c,d), and the spherical protrusions gradually change towards to the dense skeleton structure and the number of pores apparently increase. This is because of the more intensive discharge reaction which was triggered by the enhancement of the electrical conductivity with K_2ZrF_6 addition. All the details of changes can be observed from the enlarged small diagrams more clearly. According to the previous studies, silicate is considered to play the dominant role in the coating growth, and metaphosphate could promote the penetrating discharges so as to improve the compactness of the coatings [21,22]. According to the measurement results of the MAO coatings thickness, it is clear that the K_2ZrF_6 additive inhibited the deposition of silicate on the surface of coatings.

Because the thickness of the coatings changes considerably at the K_2ZrF_6 concentration of 9 g/L, here, as shown in Figure 3, the coatings prepared under the K_2ZrF_6 addition of 0 g/L and 9 g/L were

presented as the examples to explore the cross-sectional morphology and the elemental distribution. The thickness of the coatings decreases obviously with the maximum content of K_2ZrF_6 in the electrolyte, but they all have good adhesion with substrate. The coatings all exhibit a relatively dense structure with only a few micro-pores and cracks. In Figure 3b, it can be seen that the main chemical elements of the coating are consistent with the EDS results. Take the binding surface of the coating and substrate as the boundary, the content of Ti increases rapidly, while the opposite trend is observed from elements Si, P, and Zr.

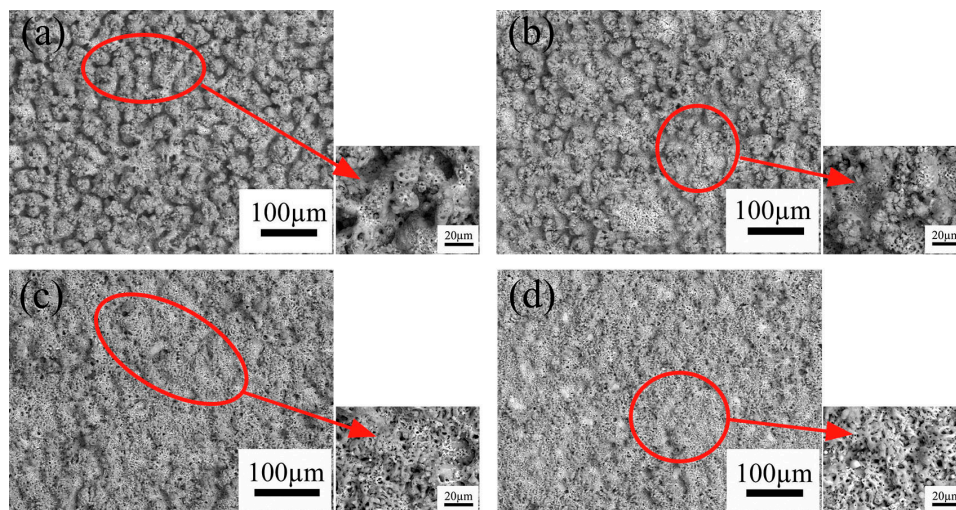


Figure 2. Surface morphologies of various MAO coatings formed in different K_2ZrF_6 concentrations: (a) 0 g/L; (b) 3 g/L; (c) 6 g/L; (d) 9 g/L.

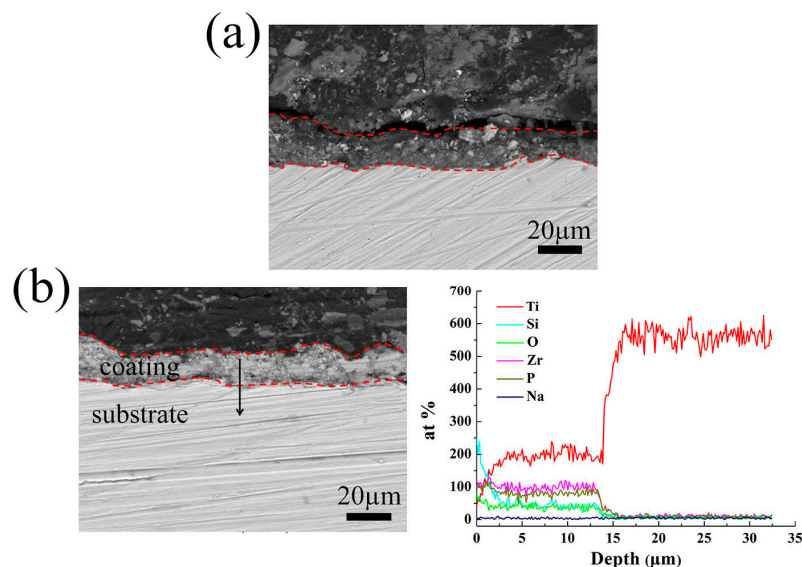


Figure 3. Cross-sectional morphologies and elemental distribution of the MAO coatings formed in different K_2ZrF_6 concentrations: (a) 0 g/L; (b) 9 g/L.

Table 1 shows the elemental distribution developed on the coatings surface of Figure 2. Generally speaking, the type and content of the elements in coatings are closely related to the composition of the electrolyte. It can be seen that the elements O, Si, P, Ti, Zr are the main content compared with other elements in the coatings. When the concentration of K_2ZrF_6 increases from 0 g/L to 9 g/L, while the content of Si element decreases quickly from 19.29% to 10.81%. Consequently, it can be concluded

that the MAO coatings were mainly formed by the deposition of silicate compounds and the K_2ZrF_6 additive evidently inhibited this deposition which provides the basis to explain the changes of the surface morphologies. In contrast, the content of P, Ti, Zr slightly increases. The increase of Zr content is due to the increase of K_2ZrF_6 addition in the electrolyte, while the increase content of elements P and Ti is because of the enhancement of the oxidation process.

Table 1. Element content of MAO coatings prepared under different K_2ZrF_6 concentrations.

K_2ZrF_6 Concentration (g/L)	Element Content of MAO Coatings (at%)							
	O	Na	Si	P	Ti	K	F	Zr
0	71.59	1.41	19.29	2.31	5.39	-	-	-
3	71.97	0.82	18.62	2.54	5.58	0.12	0.10	0.25
6	72.94	0.30	12.15	4.44	7.19	0.10	0.34	2.52
9	72.44	0.30	10.81	4.71	6.60	0.10	1.17	3.87

3.2. Phase Composition

Figure 4 shows the XRD patterns of the prepared coatings at various K_2ZrF_6 concentrations. It can be observed that the coatings are composed of anatase- TiO_2 , rutile- TiO_2 , brookite- TiO_2 and Ti. Many researchers have suggested that the reaction between (OH^-) ions and (Ti^{4+}) ions in the discharge channel could be able to form TiO_2 phases of different types [9–13,15–17,21]. Peaks conformed to Ti substrate appeared because the testing depth was higher than the thickness of the coatings. From the XRD pattern, it can also be seen that when the concentration of K_2ZrF_6 reaches 9 g/L, the peak of brookite- TiO_2 can be detected and the presence is probably due to the temperature changing during the reaction process. Brookite- TiO_2 has lower reflectivity compared to anatase- TiO_2 and rutile- TiO_2 , which could make a negative impact on the infrared emissivity of the coatings. In addition, no peaks corresponding to Zr-related, Si-related and P-related species were observed. It is deduced that these groups possibly existed as the amorphous phase. With the increase of K_2ZrF_6 addition, all the diffraction peaks become sharper and the radian of the steamed bread peak is gradually weakened, which indicated that the crystallinity of the samples tends to be better.

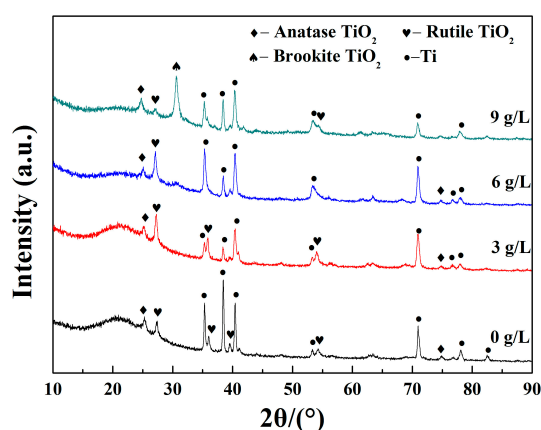


Figure 4. X-ray diffraction (XRD) patterns of MAO coatings formed under various K_2ZrF_6 concentrations.

The XPS measurement was employed to confirm the chemical composition of the MAO coatings. A clean coating surface was obtained by sputtering with Ar ions for 2 min before testing. In addition, the binding energies of all elements were corrected in reference to the C 1s peak at 284.6 eV. The survey spectrum of the coating prepared in the electrolyte of 6 g/L K_2ZrF_6 and its high-resolution spectra of major elements are shown in Figure 5. The survey spectrum discloses that the major elements in coatings are O, P, Si, Zr, Ti, Na, which is consistent with the EDS results. The C 1s spectrum shows

three peaks C-C, C-O and C=O at the bonding energy 284.6 eV, 286.1 eV and 288.8 eV respectively [23]. The O 1s spectrum can be divided into two peaks at 532.5 eV and 530.8 eV, the first peak is assigned to the Si-O bond of SiO₂ [24], while the second peak at 530.8 eV relates to O²⁻ [25,26], which corresponds with the oxides in the coatings. Two peaks of Ti 2p spectrum which are located at 464.8 eV and 458.9 eV assert the existence of TiO₂ [27]. The Si 2p spectrum exhibits two peaks at the bonding energy 102.8 eV and 103.4 eV, the peak at 103.4 eV corresponds to SiO₂, the second peak at 102.8 eV is attributed to ZrSiO₄ [28,29], the appearance of ZrSiO₄ indicates the more complex reactions in the preparation process. P 2p peaks are well fitted at 133.4 and 134.1 eV, which represent the PO₃⁻ and P₂O₇⁴⁻ separately. The ratio of the area of the two peaks is 50.27:49.73, and therefore indicates that half of the PO₃⁻ has converted to P₂O₇⁴⁻ [30,31]. The Zr 3d3/2 peak at 185.3 eV and Zr 3d5/2 peak at 182.9 eV are assigned to ZrO₂ [32]. Combined with the results of EDS, XRD and XPS, the elements Si, P, Zr were all involved in the growth of the coatings and existed in the amorphous state.

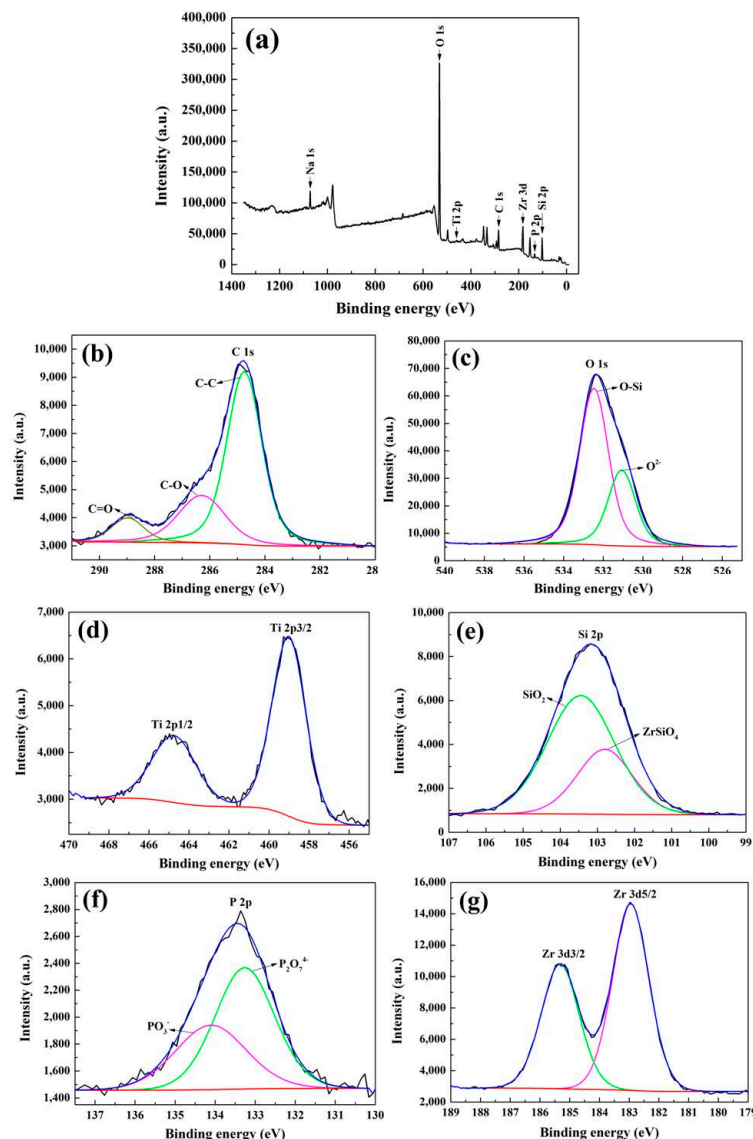


Figure 5. X-ray photoelectron spectroscopy (XPS) spectra of MAO coatings prepared with K₂ZrF₆ concentrations of 6 g/L: (a) Survey; (b) C 1s; (c) O 1s; (d) Ti 2p; (e) Si 2p; (f) P 2p; (g) Zr 3d.

3.3. Infrared Emissivity Characterization

The emissivity is a property which characterizes the radiation properties of the objects, it reveals the radiation radiates by the given body as compared with a blackbody. Higher emissivity is beneficial to the objects for their application in the field of radiative thermal protection. Figure 6 shows infrared emissivity curves measured in the wavelength of 7–20 μm of the as-prepared coatings. According to Figure 6, the coatings formed in the electrolytes added with K_2ZrF_6 have obviously higher infrared emissivity compared with the coating without K_2ZrF_6 addition. It is also found that all the coatings exhibit a higher and more stable infrared emissivity value after the wavelength of 8 μm . Therefore, the average infrared emissivity of the samples was calculated by the integration method in the wavelength of 8–20 μm and then the ratio was calculated and compared to the blackbody in the same waveband; the result is shown in Figure 7. It can be seen that the average infrared emissivity curves of the coatings present the tendency of increasing firstly and then decreasing slightly. When the concentration of K_2ZrF_6 is 6 g/L, the infrared emissivity reaches the maximum and the average infrared emissivity value is 0.89.

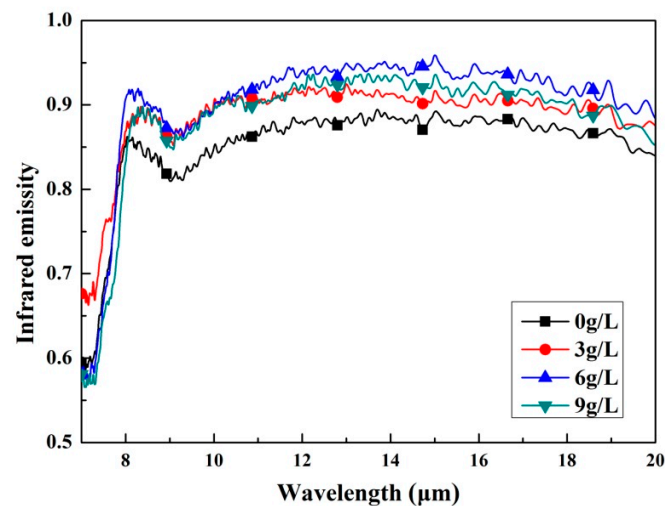


Figure 6. Infrared emissivity curves of the MAO coatings with different K_2ZrF_6 concentrations within a waveband of 7–20 μm .

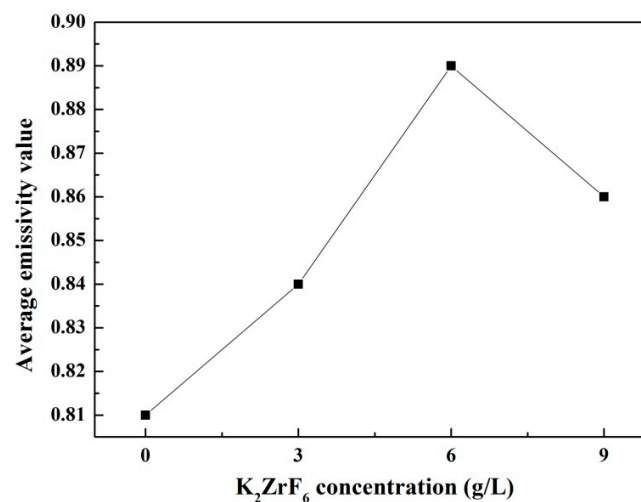


Figure 7. Average infrared emissivity curves of the MAO coatings under different K_2ZrF_6 concentrations.

The infrared emissivity value of MAO coatings can be affected by a series of factors, such as thickness, surface roughness, chemical composition and structure [33]. In general, the infrared emissivity increases with the increases of thickness and surface roughness, but the test results did not find a similar regularity. The main reason for this phenomenon is that the effect of chemical composition and structure is much greater than that of thickness and roughness. Therefore, the improvement of infrared emissivity is dependent on the addition of K_2ZrF_6 in the electrolyte. In terms of chemical composition, K_2ZrF_6 existed as the form of ZrO_2 in the MAO coatings according to the XPS results. As a kind of transition metal oxide, ZrO_2 itself has high infrared emissivity which can increase the infrared emissivity of the coatings directly. For the internal crystal structure, the lattice defects caused by the Zr^{4+} doping effect is an effective way to promote the lattice vibration, which results in the improvement of the infrared emissivity in the long wavebands. Furthermore, most groups existed in an amorphous state and the disorder of this structure leads to the formation of the local energy levels at amorphous region. The electrons could achieve the transition easily in these local energy levels, resulting in the increase of the infrared emissivity in the short wavebands [34]. When the K_2ZrF_6 concentration is 9 g/L, the slight decrease of the infrared emissivity may be due to the formation of brookite- TiO_2 and the improvement of the crystallization of the coatings [35].

4. Discussion

In short, micro arc oxidation is a complex process, the changes in the composition of the electrolyte and the change of the process parameters will have a significant effect on the reaction. According to the above presence of compound peaks in the coatings, the reaction between the TC4 substrate and electrolyte are interpreted as follows:



The reactions (1) and (2) are achieved by the oxidation of the TC4 substrate. While the reaction (2) is the main reason to promote the silicate deposition, it should be noted that the SiO_2 existed in the coatings steadily in the form of amorphous state.



Corresponding to the reaction (3), the PO_3^- ions produced by the hydrolysis of $(NaPO_3)_6$ will convert to $P_2O_7^{4-}$ at high temperature over 800 °C, and it was easy to combine with Na^+ ions in the solution to form $Na_4P_2O_7$ according to Hou's research [31].



Because of the existence of K_2ZrF_6 and NaOH in the solution, the $Zr(OH)_4$ colloid precipitation was formed through the chemical reaction between Zr^{4+} and OH^- . Then the $Zr(OH)_4$ could be dehydrated to form ZrO_2 during the sintering of the MAO process [36,37]. A series of transformations occurred through the routes of reaction (4) and (5). By considering the $ZrSiO_4$ which identified in the XPS spectra, the reaction (6) deduces the formation of Zr-Si-O species in the electrolyte under the high temperature and high pressure [38,39].

The prepared coatings can be applied to the thermal protection system (TPS) [40], which prevents the heat transferring inward and thus protects the electron apparatus. It is especially applicable for radiating the high friction heat between the aircraft surface and atmosphere and increasing the lifetime of the space vehicles material. However, the MAO coatings maybe cracked and dropped during the

extreme environment of high temperature and high pressure. The property of the coatings is affected by many factors in the process of MAO, how to keep or improve the stability and bond strength of the coatings has become a problem to be researched in future applications.

5. Conclusions

In this study, MAO coatings were successfully formed on the TC4 alloy in $\text{Na}_2\text{SiO}_3\text{-(NaPO}_3)_6$ based solution with various K_2ZrF_6 concentrations. The main results of the present survey are as follows:

1. With the increase of K_2ZrF_6 concentration, the surface morphologies of the coatings were changed to dense network structure and the number of discharge holes was significantly increased. The decrease of the thickness and the surface roughness also indicated that K_2ZrF_6 inhibited the deposition of silicate on the coatings surface.
2. From the XRD analysis, the main phases in the coatings were anatase- TiO_2 , rutile- TiO_2 together with Ti phases. The absence of any Si-based, P-based and Zr-based species in the XRD peaks identification and the high-resolution spectra of XPS further confirmed that the elements Si, P and Zr existed in the form of amorphous phase.
3. The infrared emissivity was drastically improved when the K_2ZrF_6 was added in the electrolyte. In addition, its highest value was found for the coating with the K_2ZrF_6 concentration of 6 g/L and the average could reach 0.89 at wavelength of 8–20 μm . It is considered that the doping of Zr^{4+} and the formation of amorphous ZrO_2 enhanced the infrared emissivity of the coatings.

Acknowledgments: This work was financially supported by the Natural Science Foundation of China (Grant No. 51474057 and 51274057).

Author Contributions: Guangrui Gao and Ying Li conceived and designed the experiments; Dan Hu carried out the experiments; Guangrui Gao and Dan Hu analyzed the experimental results and wrote this paper; Zhengping Xi analyzed the infrared emissivity characterization of the samples; Ying Li read and approved the manuscript.

Conflicts of Interest: The authors declare no conflict of interest.

References

1. Tang, H.; Sun, Q.; Yi, C.G.; Jiang, Z.H.; Wang, F.P. High emissivity coatings on titanium alloy prepared by micro-arc oxidation for high temperature application. *J. Mater. Sci.* **2012**, *47*, 2162–2168. [[CrossRef](#)]
2. Tang, H.; Sun, Q.; Xin, T.Z.; Yi, C.G.; Jiang, Z.H.; Wang, F.P. Influence of $\text{Co}(\text{CH}_3\text{COO})_2$ concentration on thermal emissivity of coatings formed on titanium alloy by micro-arc oxidation. *Curr. Appl. Phys.* **2012**, *12*, 284–290. [[CrossRef](#)]
3. Rodríguez-Barrero, S.; Fernández-Larrinoa, J.; Azkona, I.; Lacalle, L.N.L.D.; Polvorosa, R. Enhanced Performance of Nanostructured Coatings for Drilling by Droplet Elimination. *Mater. Manuf. Process.* **2014**, *31*, 1–10. [[CrossRef](#)]
4. Polvorosa, R.; Suárez, A.; Lacalle, L.N.L.D.; Cerrillo, I.; Wretland, A.; Veiga, F. Tool wear on nickel alloys with different coolant pressures: Comparison of Alloy 718 and Waspaloy. *J. Manuf. Process.* **2017**, *26*, 44–56. [[CrossRef](#)]
5. Fernández-Abia, A.I.; Barreiro, J.; Lacalle, L.N.L.D.; González-Madruga, D. Effect of mechanical pre-treatments in the behaviour of nanostructured PVD-coated tools in turning. *Int. J. Adv. Manuf. Technol.* **2014**, *73*, 1119–1132. [[CrossRef](#)]
6. Ge, Y.L.; Wang, Y.M.; Zhang, Y.F.; Guo, L.X.; Jia, D.C.; Ouyang, J.H.; Zhou, Y. The improved thermal radiation property of SiC doped micro arc oxidation ceramic coating formed on niobium metal for metal thermal protective system. *Surf. Coat. Technol.* **2017**, *309*, 880–886. [[CrossRef](#)]
7. Hong, Z.L.; Ouyang, J.H.; Liu, Z.G.; Wang, Y.M. Microstructure, thermal shock resistance and thermal emissivity of plasma sprayed $\text{La}_M\text{Al}_{11}\text{O}_{19}$ ($M = \text{Mg}, \text{Fe}$) coatings for metallic thermal protection systems. *Appl. Surf. Sci.* **2013**, *271*, 52–59. [[CrossRef](#)]
8. Li, Z.; Zheng, F.; Gong, H.Q.; Hu, P.F.; Song, S.L.; Zhen, Q. Study on ZrSiO_4 -aluminosilicate glass coating with high infrared emissivity and anti-oxidation properties. *Compos. Commun.* **2017**, *4*, 16–19. [[CrossRef](#)]

9. Tang, H.; Xin, T.Z.; Sun, Q.; Yi, C.G.; Jiang, Z.H.; Wang, F.P. Influence of FeSO_4 concentration on thermal emissivity of coatings formed on titanium alloy by micro-arc oxidation. *Appl. Surf. Sci.* **2011**, *257*, 10839–10844. [[CrossRef](#)]
10. Karbowniczek, J.; Muhaffel, F.; Cempura, G.; Cimenoglu, H.; Filemonowicz, A.C. Influence of electrolyte composition on microstructure, adhesion and bioactivity of micro-arc oxidation coatings produced on biomedical Ti6Al7Nb alloy. *Surf. Coat. Technol.* **2017**, *321*, 97–107. [[CrossRef](#)]
11. Wang, Y.H.; Liu, Z.G.; Ouyang, J.H.; Wang, Y.M.; Zhou, Y. Influence of electrolyte compositions on structure and high-temperature oxidation resistance of microarc oxidation coatings formed on Ti2AlNb alloy. *J. Alloys Compd.* **2015**, *647*, 431–437. [[CrossRef](#)]
12. Qiao, L.P.; Lou, J.; Zhang, S.F.; Qu, B.; Chang, W.H.; Zhang, R.F. The entrance mechanism of calcium and phosphorus elements into micro arc oxidation coatings developed on Ti6Al4V alloy. *Surf. Coat. Technol.* **2016**, *285*, 187–196. [[CrossRef](#)]
13. Xu, Y.J.; Yao, Z.P.; Jia, F.Z.; Wang, Y.L.; Jiang, Z.H.; Bu, H.T. Preparation of PEO ceramic coating on Ti alloy and its high temperature oxidation resistance. *Curr. Appl. Phys.* **2010**, *10*, 698–702. [[CrossRef](#)]
14. Ezhilselvi, V.; Nithin, J.; Balaraju, J.N.; Subramanian, S. The influence of current density on the morphology and corrosion properties of MAO coatings on AZ31B magnesium alloy. *Surf. Coat. Technol.* **2016**, *288*, 221–229. [[CrossRef](#)]
15. Zhang, X.M.; Chen, D.F.; Gong, X.Z.; Yang, S.Q.; Tian, X.B. Modulation effects of K_2ZrF_6 additive on microstructure and heat resistance of micro-arc oxide coatings fabricated on LY12 aluminum alloy. *J. Inorg. Mater.* **2010**, *25*, 865–870. [[CrossRef](#)]
16. Liang, J.; Guo, B.G.; Tian, J.; Liu, H.W.; Zhou, J.F.; Xu, T. Effect of potassium fluoride in electrolytic solution on the structure and properties of microarc oxidation coatings on magnesium alloy. *Appl. Surf. Sci.* **2005**, *252*, 345–351. [[CrossRef](#)]
17. Wang, Z.; Wu, L.; Cai, W.; Shan, A.; Jiang, Z.H. Effects of fluoride on the structure and properties of microarc oxidation coating on aluminium alloy. *J. Alloys Compd.* **2010**, *505*, 188–193. [[CrossRef](#)]
18. Kang, M.L.; Ko, Y.G.; Dong, H.S. Microstructural characteristics of oxide layers formed on Mg–9 wt % Al–1 wt % Zn alloy via two-step plasma electrolytic oxidation. *J. Alloys Compd.* **2014**, *615*, S418–S422. [[CrossRef](#)]
19. Tsunekawa, S.; Aoki, Y.; Habazaki, H. Two-step plasma electrolytic oxidation of Ti–15V–3Al–3Cr–3Sn for wear-resistant and adhesive coating. *Surf. Coat. Technol.* **2011**, *205*, 4732–4740. [[CrossRef](#)]
20. Einkhah, F.; Kang, M.L.; Sani, M.A.F.; Yoo, B.; Dong, H.S. Structure and corrosion behavior of oxide layer with Zr compounds on AZ31 Mg alloy processed by two-step plasma electrolytic oxidation. *Surf. Coat. Technol.* **2014**, *238*, 75–79. [[CrossRef](#)]
21. Li, Q.B.; Yang, W.B.; Liu, C.C.; Wang, D.A.; Liang, J. Correlations between the growth mechanism and properties of micro-arc oxidation coatings on titanium alloy: Effects of electrolytes. *Surf. Coat. Technol.* **2017**, *316*, 162–170. [[CrossRef](#)]
22. Ma, H.; Li, D.; Liu, C.; Huang, Z.; He, D.; Yan, Q.; Liu, P.; Nash, P.; Shen, D.J. An investigation of $(\text{NaPO}_3)_6$ effects and mechanisms during micro-arc oxidation of AZ31 magnesium alloy. *Surf. Coat. Technol.* **2015**, *266*, 151–159. [[CrossRef](#)]
23. Zhu, X.L.; Chen, J.; Scheideler, L.; Reichl, R.; Geis-Gerstorfer, J. Effects of topography and composition of titanium surface oxides on osteoblast responses. *Biomaterials* **2004**, *25*, 4087–4103. [[CrossRef](#)] [[PubMed](#)]
24. Dang, T.A.; Chou, C.N. Electron spectroscopy for chemical analysis of cool white phosphors coated with SiO_2 thin film. *J. Electrochem. Soc.* **1996**, *143*, 302–305. [[CrossRef](#)]
25. Li, S.J.; Yang, R.; Niinomi, M.; Hao, Y.L.; Cui, Y.Y. Formation and growth of calcium phosphate on the surface of oxidized Ti–29Nb–13Ta–4.6Zr alloy. *Biomaterials* **2004**, *25*, 2525–2532. [[CrossRef](#)] [[PubMed](#)]
26. Kaciulis, S.; Mattogno, G.; Napoli, A.; Bemporad, E.; Ferrari, F.; Montenero, A.; Gnappi, G. Surface analysis of biocompatible coatings on titanium. *J. Electron Spectrosc. Relat. Phenom.* **1998**, *95*, 61–69. [[CrossRef](#)]
27. Santos, A.D.; Araujo, J.R.; Landi, S.M.; Kuznetsov, A.; Granjeiro, J.M.; Sena, L.A.D.; Achete, C.A. A study of the physical, chemical and biological properties of TiO_2 coatings produced by micro-arc oxidation in a Ca-P-based electrolyte. *J. Mater. Sci. Mater. Med.* **2014**, *25*, 1769–1780. [[CrossRef](#)] [[PubMed](#)]
28. Moulder, J.F.; Stickle, W.F.; Sobol, P.E.; Bomben, K.D. *Handbook of X-ray Photoelectron Spectroscopy*; Perkin-Elmer Corporation: Eden Prairie, MN, USA, 1992.
29. Dementjev, A.P.; Ivanova, O.P.; Vasilyev, L.A.; Naumkin, A.V.; Nemirovsky, D.M.; Shalaev, D.Y. Altered layer as sensitive initial chemical state indicator. *J. Vac. Sci. Technol. A Vac. Surf. Films* **1994**, *12*, 423–425. [[CrossRef](#)]

30. Shokouhfar, M.; Allahkaram, S.R. Formation mechanism and surface characterization of ceramic composite coatings on pure titanium prepared by micro-arc oxidation in electrolytes containing nanoparticles. *Surf. Coat. Technol.* **2016**, *291*, 396–405. [[CrossRef](#)]
31. Kok, W.H.; Sun, X.; Shi, L.; Wong, K.; Mitchell, K.A.R.; Foster, T. Formation of zinc phosphate coatings on AA6061 aluminum alloy. *J. Mater. Sci.* **2001**, *36*, 3941–3946. [[CrossRef](#)]
32. Okazaki, Y.; Tateishi, T.; Ito, Y. Corrosion resistance of implant alloys in pseudo physiological solution and role of alloying elements in passive films. *Mater. Trans. JIM* **1997**, *38*, 78–84. [[CrossRef](#)]
33. Huang, Z.; Zhou, W.; Tang, X.; Zhu, D.; Luo, F. Effects of substrate roughness on infrared-emissivity characteristics of Au films deposited on Ni alloy. *Thin Solid Films* **2011**, *519*, 3100–3106. [[CrossRef](#)]
34. Cheng, X.D.; Min, J.; Zhu, Z.Q.; Ye, W.P. Preparation of high emissivity NiCr₂O₄ powders with a spinel structure by spray drying. *Int. J. Miner. Metall. Mater.* **2012**, *19*, 173–178. [[CrossRef](#)]
35. Chen, X.B.; Liu, L.; Yu, P.Y.; Mao, S.S. Increasing solar absorption for photocatalysis with black hydrogenated titanium dioxide nanocrystals. *Science* **2011**, *331*, 746–750. [[CrossRef](#)] [[PubMed](#)]
36. Durdu, S.; Bayramoglu, S.; Demirtas, A.; Usta, M.; Ucisik, A.H. Characterization of AZ31 Mg Alloy coated by plasma electrolytic oxidation. *Vacuum* **2013**, *88*, 130–133. [[CrossRef](#)]
37. Zhang, R.F.; Zhang, S.F.; Xiang, J.H.; Zhang, L.H.; Zhang, Y.Q.; Guo, S.B. Influence of sodium silicate concentration on properties of micro arc oxidation coatings formed on AZ91HP magnesium alloys. *Surf. Coat. Technol.* **2012**, *206*, 5072–5079. [[CrossRef](#)]
38. Rehman, Z.U.; Shin, S.H.; Lim, H.T.; Koo, B.H. Transformation of plasma electrolytic oxidation coatings from crater to cluster-based structure with increase in DC voltage and the role of ZrO₂ nanoparticles. *Surf. Coat. Technol.* **2017**, *311*, 383–390. [[CrossRef](#)]
39. Rehman, Z.U.; Shin, S.H.; Hussain, I.; Koo, B.H. Structure and corrosion properties of the two-step PEO coatings formed on AZ91D Mg alloy in K₂ZrF₆-based electrolyte solution. *Surf. Coat. Technol.* **2016**, *307*, 484–490. [[CrossRef](#)]
40. Fernández-Abia, A.I.; Barreiro, J.; Lacalle, L.N.L.D.; Martínez-Pellitero, S. Behavior of austenitic stainless steels at high speed turning using specific force coefficients. *Int. J. Adv. Manuf. Technol.* **2012**, *62*, 505–515. [[CrossRef](#)]



© 2018 by the authors. Licensee MDPI, Basel, Switzerland. This article is an open access article distributed under the terms and conditions of the Creative Commons Attribution (CC BY) license (<http://creativecommons.org/licenses/by/4.0/>).